Chemistry & Biology
Article

Structural Characterization of Acylimine-Containing Blue and Red Chromophores in mTagBFP and TagRFP Fluorescent Proteins

Oksana M. Subach,[1,3] Vladimir N. Malashkevich,[2,3] Wendy D. Zencheck,[2] Kateryna S. Morozova,[1] Kiryl D. Piatkevich,[1] Steven C. Almo,[2] and Vladislav V. Verkhusha[1,*]
[1]Department of Anatomy and Structural Biology and Gruss-Lipper Biophotonics Center
[2]Department of Biochemistry
Albert Einstein College of Medicine, 1300 Morris Park Avenue, Bronx, NY10461, USA
[3]These authors contributed equally to this work
*Correspondence: vladislav.verkhusha@einstein.yu.edu
DOI 10.1016/j.chembiol.2010.03.005

SUMMARY

We determined the 2.2 Å crystal structures of the red fluorescent protein TagRFP and its derivative, the blue fluorescent protein mTagBFP. The crystallographic analysis is consistent with a model in which TagRFP has the *trans* coplanar anionic chromophore with the conjugated π-electron system, similar to that of DsRed-like chromophores. Refined conformation of mTagBFP suggests the presence of an N-acylimine functionality in its chromophore and single C^{α}-C^{β} bond in the Tyr64 side chain. Mass spectrum of mTagBFP chromophore-bearing peptide indicates a loss of 20 Da upon maturation, whereas tandem mass spectrometry reveals that the C^{α}-N bond in Leu63 is oxidized. These data indicate that mTagBFP has a new type of the chromophore, *N*-[(5-hydroxy-1*H*-imidazole-2-yl)methylidene]acetamide. We propose a chemical mechanism in which the DsRed-like chromophore is formed via the mTagBFP-like blue intermediate.

INTRODUCTION

Crystal structures for a number of green fluorescent protein (GFP)–like proteins, including fluorescent proteins (FPs) and absorbing but nonfluorescent chromoproteins (CPs), have been reported (Stepanenko et al., 2008). Chromophores in both FPs and CPs result from the spontaneous cyclization of X-Tyr-Gly tripeptides (where X represents any amino acid) inside the characteristic 11-stranded β-barrel. Chromophore formation is an autocatalytic process that only requires molecular oxygen. The green-emitting tyrosine-based chromophore consists of an anionic conjugate of imidazolone with p-hydroxybenzylidene (Ormö et al., 1996). Chromophore protonation results in an absorbance shift to ~400 nm (Brejc et al., 1997). Blue and cyan color variants of GFP contain the substitutions of tyrosine in the chromophore with histidine and tryptophan (Heim and Tsien, 1996; Heim et al., 1994). In red tyrosine-based chromophores, such as in the one observed in DsRed (Yarbrough et al., 2001), the peptide bond, which precedes the first amino acid in the chromophore tripeptide, is oxidized. The oxidation reaction yields an N-acylimine derivative that results in an extended π-system conjugation and a shift of the absorbance and emission spectra to the red (Yarbrough et al., 2001).

The majority of FPs exhibits a *cis* chromophore configuration with the hydroxyphenyl ring coplanar to the imidazolone ring and pointing away from its carbonyl group (Ormö et al., 1996; Yarbrough et al., 2001). Weakly fluorescent FPs and CPs, in turn, have the hydroxyphenyl ring in a *trans* configuration—that is, pointing toward a carbonyl group of the imidazolone ring—and exhibit a noncoplanar conformation relative to the imidazolone ring (Prescott et al., 2003). The only known FP featuring a *trans* coplanar chromophore is eqFP611 (Petersen et al., 2003).

A detailed maturation mechanism for the chromophores of red FPs (RFPs) remains unknown (Piatkevich and Verkhusha, 2010). It has been suggested, however, that formation of the DsRed red chromophore proceeds via a green GFP-like immature intermediate (Gross et al., 2000). In contrast, our group proposed that the DsRed chromophore can be formed from a blue protonated chromophore intermediate with an absorbance maximum at ~400 nm, but not from the anionic GFP-like chromophore, which is a dead-end product (Verkhusha et al., 2004). Absorbance at ~400 nm has also been observed in immature species of many red-shifted CPs, including asulCP, cgigCP, hcriCP, and HcRed1 (Verkhusha et al., 2004; Wilmann et al., 2005). Previously, we have successfully applied a rational mutagenesis to five genetically unrelated RFPs, such as TagRFP (Merzlyak et al., 2007), mCherry (Shu et al., 2006), HcRed1 (Wilmann et al., 2005), M355NA (Bulina et al., 2003), and mKeima (Kogure et al., 2006), in order to develop the respective mTagBFP, mCherry-blue, HcRed1-blue, M355NA-blue, and mKeima-blue blue FP (BFP) variants (Subach et al., 2008). That was achieved by introducing a limited number of the site-specific amino acid substitutions in these RFPs. Furthermore, several so-called Fluorescent Timers, which change fluorescence color from blue to red over time, have been developed on the basis of mCherry (Subach et al., 2009), and their crystal structures have been determined (Pletnev et al., 2010).

On the basis of all these data, we hypothesized that a formation pathway for a red chromophore via a blue intermediate should be

Table 1. Data Collection and Refinement Statistics

Data collection	TagRFP	mTagBFP
Beamline	NSLS-X29A	NSLS-X29A
Wavelength (Å)	1.08	1.08
Resolution limits (Å)	20–2.2	20–2.2
Observed reflections	236,532	360,436
Unique reflections	41,893	55,493
Completeness (%)	92.4 (56.0)[a]	89.1 (56.4)[a]
R_{merge}[b]	0.090 (0.472)[a]	0.068 (0.222)[a]
Refinement statistics		
Protein nonhydrogen atoms	6527	6869
Water molecules	664	402
R_{cryst}[c]	0.159 (0.387)[a]	0.195 (0.214)[a]
R_{free}[c]	0.179 (0.397)[a]	0.238 (0.277)[a]
Average B-factor (Å^2)	23.5	15.9
RMSD from ideality		
Bond length, Å	0.012	0.009
Bond angles (°)	1.68	1.29
Torsion angles (°)	21.8	23.1
Ramachandran plot		
Core (%)	93.6	94.2
Allowed (%)	5.2	4.7
Generous (%)	1.2	1.1

[a] Values in parentheses indicate statistics for the high resolution bin.
[b] $R_{merge} = \Sigma\Sigma\, j|Ij(hkl) - < I(hkl) > |/ \Sigma\Sigma\, j| < I(hkl) > |$, where Ij is the intensity measurement for reflection j and < I > is the mean intensity over j reflections.
[c] $R_{cryst}/(R_{free}) = \Sigma\, ||F_o(hkl)| - |F_c(hkl)||/ \Sigma\, |F_o(hkl)|$, where F_o and F_c are observed and calculated structure factors, respectively. No σ-cutoff was applied; 5% of the reflections were excluded from refinement and used to calculate R_{free}.

conserved, and a direct comparison of chromophores and their environments in the closely related BFP and RFP should provide insight into the pathway of the red chromophore formation. Here, we report the crystal structures of TagRFP and its derivative mTagBFP, mass-spectral data of the mTagBFP chromophore-bearing peptide, and an extensive spectral and biochemical characterization of mTagBFP mutants. These data have revealed, for the first time to our knowledge, a chemical structure of the blue acylimine–containing chromophore and allowed us to suggest a chemical pathway for chromophore transformations from the nonoxidized colorless to the blue fluorescent state, and subsequently from the blue to the red fluorescent state.

RESULTS

Overall Structures of TagRFP and mTagBFP

The final crystal structure of TagRFP was refined at a 2.2 Å resolution (Table 1). The asymmetric unit contains four TagRFP protein chains arranged into two identical dimers (AB and CD), with total solvent accessible area of 18,080 Å^2 per dimer (see Figure S1A available online). The interface area within each dimer buries 1,475 Å^2 per chain, significantly larger than the interface area of 409 Å^2 per chain between the dimers. Most of the residues of each chain (Glu3–Leu228) are well defined in the electron density map, with the exception of six N-terminal residues and five C-terminal residues of each chain, which are not visible; here and below, we follow the amino acid numbering used for eqFP611 (Petersen et al., 2003) and mKate (Pletnev et al., 2008) (see Figure S1). The four molecules in the asymmetric unit have similar overall temperature factors of 23.9, 23.9, 24.2, and 23.7 Å^2, and almost identical structures, with RMS deviations between all the C_α atoms of subunit A and three other subunits being 0.26, 0.29, and 0.14 Å, respectively.

The crystal structure of mTagBFP was refined at a 2.2 Å resolution (Table 1). The asymmetric unit contains four mTagBFP protein chains (Figure S1C), which assemble into a tetramer identical to that observed in mKate (Pletnev et al., 2008). The tetramer demonstrates 222 point symmetry, its total solvent accessible area being 32,690 Å^2 with the buried surface area of 2,240 Å^2 per chain. The interface area between the dimers is 918 Å^2 per chain, smaller than the interface of 1,450 Å^2 per chain within a dimer. Within the mTagBFP tetramer, AB and CD dimers are very similar in overall structure to the TagRFP dimers. The overall temperature factors are 12.1, 14.7, 15.2, and 22.0 Å^2 for the four molecules in the asymmetric unit. The RMS deviations between the subunit A and three other subunits are 0.24, 0.23, and 0.32 Å, respectively. The subsequent structural analysis will refer to the best defined A subunit of mTagBFP. Each chain of TagRFP and mTagBFP is folded into the characteristic 11-stranded β-barrel, described previously for GFP (Ormö et al., 1996), DsRed (Yarbrough et al., 2001), eqFP611 (Petersen et al., 2003), HcRed (Wilmann et al., 2005), and mKate (Pletnev et al., 2008), where the central chromophore-containing α-helix is extended coaxially with the axes of the β-barrel (Figures S1B and S1D). Notably, gel filtration and seminative gel electrophoresis experiments indicate that both TagRFP and mTagBFP remain monomeric in solution up to the concentration of 10 mg/ml (Merzlyak et al., 2007; Subach et al., 2008), indicating that oligomerization occurs only under very high protein concentration observed in the crystalline phase.

Chromophore Structure in TagRFP

Electron density of the TagRFP Met63-Tyr64-Gly65 tripeptide suggests the formation of a 5-[(4-hydroxyphenyl)-methylene]-imidazolone chromophore. The chemical structure is the same as in eqFP611 (Petersen et al., 2003). The electron density for Met63 can be interpreted such that C^α is characterized by sp^2 hybridization, suggesting the formation of an N-acylimine double bond between C^α and N. As in other red and far-red FPs, this additional N-acylimine may extend the π-bonding system resulting in a red shift in excitation/emission spectra. Similar to other red FPs (Yarbrough et al., 2001; Petersen et al., 2003), the Phe62-Met63 peptide bond in TagRFP has a *cis* conformation.

TagRFP has the almost coplanar *trans* chromophore with $\chi_1 = -5 \pm 4°$ and $\chi_2 = 5 \pm 4°$ (subunit A) (Figure 1A). The eqFP611 (Petersen et al., 2003) and mKate proteins at low pH (Pletnev et al., 2008) have the similar *trans* coplanar chromophore. The amino acid sequences of TagRFP and eqFP611 share 76% identity (Figure S1E). The immediate surroundings of the chromophores in these proteins are identical except for Arg67 in TagRFP, which is replaced by Lys67 in eqFP611. However, mKate carries three additional alterations in the immediate environment of the chromophore relative to TagRFP

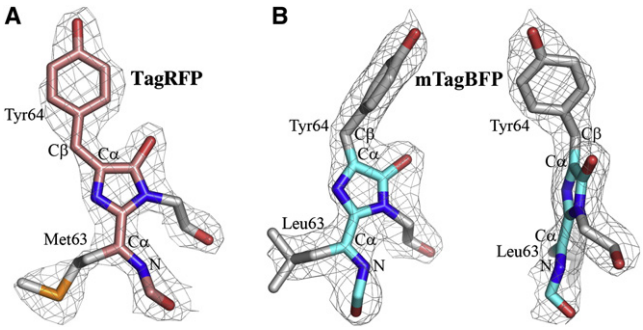

Figure 1. Structures of the Chromophore-Forming Tripeptides Superimposed Onto Their (2Fo-Fc) Electron Density Maps

(A) TagRFP, subunit A.

(B) mTagBFP, subunit A, two orthogonal views. Oxygen and nitrogen atoms are colored red and blue, respectively. The chromophore backbones for TagRFP and mTagBFP are shown in orange and cyan, respectively. See also Figure S1.

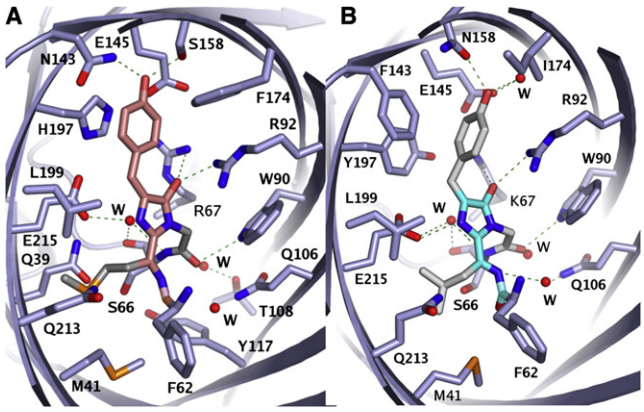

Figure 2. Chromophores and Their Environments in TagRFP and mTagBFP

The chromophore backbones for TagRFP (A) and mTagBFP (B) are shown in orange and cyan, respectively. The hydrogen bonds are indicated with green dashed lines, the atoms are colored by atom type, and the water molecules are shown as red spheres. The Ala59, Thr60, and Ser61 residues are not included for figure clarity. See also description of contacts of the TagRFP and mTagBFP chromophores with the respective β-barrel interiors in the Supplemental Information.

(Lys67, Ser143, Leu174, and Arg197 in mKate versus Arg67, Asn143, Phe174, and His197 in TagRFP), and the mKate chromophore in the fluorescent state (high pH) has a *cis* configuration. The TagRFP chromophore is involved in multiple interactions within the β-barrel interior (Figure 2A).

Chromophore Structure in mTagBFP

Electron density of mTagBFP can be interpreted as being consistent with the posttranslational modification of the chromophore-forming tripeptide Leu63-Tyr64-Gly65 that results mainly in the formation of a 4-(4-hydroxybenzyl)-1H-imidazole-5-ol chromophore. Electron density at Leu63 C^{α} suggests sp^2 hybridization, indicating that the blue fluorescent protein mTagBFP may have an N-acylimine double bond between C^{α} and N of Leu63, similar to that observed in red fluorescent proteins. Slightly diffuse electron density map might indicate a minor hydrolytic degradation of Leu63 C^{α}. The cleavage of the first residue X (in the X-Tyr-Gly) tripeptide has been recently observed in the chromophores of the fast Fluorescent Timer and its blue precursor (Pletnev et al., 2010). Similar phenomenon might also occur in mTagBFP. This degradation is not caused by radiation, since electron densities calculated with subsets from the start of data collection and from the end are almost identical. To further reveal chemical structure of the mTagBFP chromophore, we subjected the chromophore-bearing peptide to mass spectrometry analysis (see below). It confirmed the presence of the N-acylimine C = N bond in the mTagBFP chromophore. The Phe62-Leu63 peptide bond is close to the *cis* conformation that is characteristic of red FPs with the N-acylimine (Yarbrough et al., 2001; Petersen et al., 2003).

The hydroxyphenyl group of Tyr64 has the noncoplanar conformation with the $\chi_1 = 136 \pm 4^{\circ}$ and $\chi_2 = -66 \pm 4^{\circ}$ (Figure 1B). A similar noncoplanar conformation has been observed in the dark state of photoswitchable FPs, in chromoproteins and in FPs with low quantum yields (Prescott et al., 2003; Quillin et al., 2005; Wilmann et al., 2006; Stiel et al., 2007; Andresen et al., 2005). The presence of this conformation in mTagBFP is remarkable, given the high quantum yield of this FP. Because none of the torsion angles is 0 or 180°, C^{β} of Tyr64 has sp^3 hybridization. On the basis of these data, we suggest that in mTagBFP the hydroxyphenyl group of Tyr64 is not in conjugation with the imidazole ring, and that the C^{α}-C^{β} bond of the Tyr64 is fully reduced. At the same time, the electron density of mTagBFP suggests that the C^{α} atom of Tyr64 has mainly planar geometry. In this conformation, the imidazole ring is coplanar with the C = N bond of the acylimine in all four molecules of the asymmetric unit. This finding is consistent with the aromatic character of the imidazole ring and suggests sp^2 hybridization of Tyr64 C^{α}. We cannot exclude, however, that there may be an alternative conformation of the chromophore, in which the imidazolone ring is present. Because the mTagBFP crystal structure mainly shows the planar geometry of the imidazole ring, the keto-enol equilibrium between imidazolone and imidazole-5-ol is shifted toward the imidazole-5-ol heterocycle. This shift possibly occurs because the delocalization of electron density in the aromatic imidazole-5-ol system is more energetically advantageous than that in the nonaromatic (nonconjugated) imidazolone ring. The mTagBFP chromophore is involved in multiple interactions within the β-barrel interior (Figure 2B). Contacts of the TagRFP and mTagBFP chromophore-tripeptides with the respective β-barrel interiors are described in the Supplemental Information.

Spectral Properties of TagRFP and mTagBFP

Spectral variety of FPs is determined by different types of chromophores but also by chromophore interactions with the surrounding amino acids within the β-barrels. After denaturation in acid or alkali, absorbance spectrum reflects the type of the chromophore structure free from interactions with other residues. In acidic conditions (0.2 M HCl), TagRFP showed a single maximum at 387 nm. In alkaline conditions (0.7 M NaOH), it had a single maximum at 449 nm (Figure 3A). These spectral forms of the denatured TagRFP were interconvertible, with a change in conditions from acidic to alkaline and vice versa. The maxima

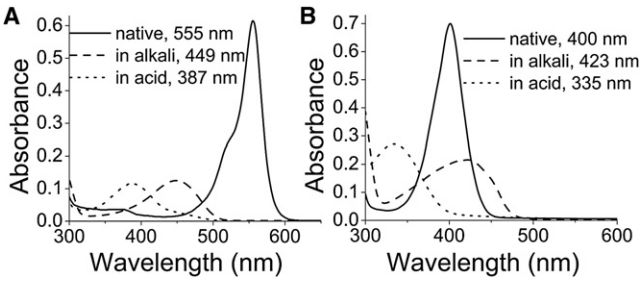

Figure 3. Absorbance Spectra of TagRFP and mTagBFP
Spectra for TagRFP (A) and mTagBFP (B) are shown in PBS buffer (solid lines), denatured in 0.7 M NaOH (dashed lines), and denatured in 0.2 M HCl (dotted lines).

were similar to those observed for GFP in acid and alkali (Niwa et al., 1996). The DsRed-like chromophore in TagRFP converted into the GFP-like chromophore under acidic or alkaline conditions. Possibly, a hydration of the N-acylimine C = N bond in the TagRFP chromophore has occurred. Similar hydration of the acylimine bond has been observed for the chromophores in DsRed itself (Gross et al., 2000) and in gtCP (Martynov et al., 2003). In contrast, mTagBFP exhibited a single absorbance maximum at 335 nm in acid, and single maximum at 423 nm in alkali (Figure 3B). The mTagBFP forms, corresponding to these maxima, converted to each other with a change of the pH conditions as well. The maxima differed from those for GFP in acidic and alkaline conditions (Niwa et al., 1996). These data suggested that mTagBFP contains a non-GFP-like and non-DsRed-like chromophore.

Mutants of mTagBFP Affecting Chromophore Formation

To study properties of the chromophore structure in mTagBFP, a site-directed mutagenesis of the amino acid residues of the chromophore-forming tripeptide and of its immediate environment was performed next.

Position 64

To test whether a side chain of Tyr64 is necessary for the formation of the mTagBFP chromophore, we first substituted Tyr64 with several aliphatic residues such as Leu, Val, Ala, and Gln. The substitution resulted in blue-emitting FP variants with the absorbance maxima at 398–400 nm and the emission maxima at 453–459 nm, which were very similar to those observed for mTagBFP (Table 2; Figures S2A–S2E). The spectral data suggested that Tyr64 in mTagBFP does not form a C^{α}-C^{β} double bond and, therefore, the side chain of Tyr64 is not involved in the conjugation with the imidazole-5-ol residue.

Position 143

According to the mTagBFP crystal structure, the hydroxyphenyl group of Tyr64 is noncoplanar with the imidazole-5-ol. This occurs because the bulky side chain of Phe143 pushes the hydroxyphenyl group out of plane of the imidazole-5-ol ring. The Phe143Ser substitution resulted in the mutant with three absorbance maxima: at 395, 515, and 582 nm (Table 2; Figure S2F). Excitation of the mTagBFP/F143S mutant at 395 and 582 nm resulted in fluorescence with maxima at 462 and 631 nm, respectively (Table 2; Figure S2F). At the same time, the mTagBFP/F143S mutant showed a single absorbance maximum in acidic (at 383 nm) or alkaline (at 447 nm) conditions. Both absorbance maxima are characteristic of the GFP-like (Niwa et al., 1996) and DsRed-like (Gross et al., 2000) chromophores. The data suggest that the 395, 515, and 581 nm mTagBFP/F143S forms correspond to the protonated and anionic states of GFP-like chromophore and DsRed-like chromophore, respectively. Because absorbance and fluorescence maxima of the mTagBFP/F143S are at 581 and 631 nm, respectively, its DsRed-like chromophore possibly has a *cis* configuration similar to that of mKate (Pletnev et al., 2008). Apparently, Ser143 in the mTagBFP/F143S stabilizes the *cis* configuration of its chromophore. At the same time, Ser158 in TagRFP stabilizes the *trans* configuration of its chromophore. Thus, the

Table 2. Spectral Properties of the mTagBFP Mutants

mTagBFP mutant	Absorbance maximum in PBS, nm	Absorbance maximum in 0.7 M NaOH, nm	Absorbance maximum in 0.2 M HCl, nm	Fluorescence maximum, nm (excitation at 400 nm)	Extinction coefficient, M^{-1} cm^{-1}	Quantum yield	Brightness relative to mTagBFP, %[a]
mTagBFP	400	423	335	455	52,000	0.63	100
Y64L	399	ND[b]	ND	459	22,000	0.68	46
Y64V	400	ND	ND	457	13,000	0.68	27
Y64A	398	ND	ND	453	6,000	0.47	9
Y64Q	399	ND	ND	457	23,000	0.77	54
F143S	395, 515, 581	447	383	462	5,000	0.01	2
				631[c]	11,000	0.003	0.4[d]
S66A	400	419	ND	456	6,000	0.22	4
Q106L	380, 400	379, 428	ND	452	2,000	0.20	1
E215A	386	ND	ND	Not detectable	~0	~0	~0

See also Figure S2.
[a] Brightness of mTagBFP mutants was determined as a product of quantum yield and extinction coefficient and normalized to the brightness of mTagBFP, which was assumed 100%.
[b] ND, not determined.
[c] Fluorescence maximum at 631 nm was obtained with excitation at 581 nm.
[d] Brightness relative to mKate.

mTagBFP peptide LYGSKTF
m/z predicted 815.43
m/z observed 795.4
Δ*m/z* 20 Da

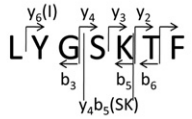

Assignment	*m/z* calculated	*m/z* observed
y_4b_5(SK)	215.13	216.17
y_2	267.13	267.18
b_3	314.15	314.18
y_3	395.23	395.26
y_4	482.26	482.29
b_5	529.28	529.30
b_6	630.33	630.35
i	710.32	710.34

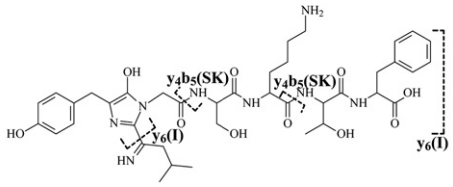

Figure 4. Mass-Spectral Analysis of the Chromophore-Bearing Peptide of mTagBFP

Table representing the distinctive peaks in MS/MS spectra of the chromophore-bearing peptide ions and structure of the mTagBFP chymotrypsin-derived chromopeptide are shown. The most prominent MS/MS fragments are presented in brackets.

Phe143 bulky side chain sterically inhibits oxidation of the C^{α}-C^{β} bond in the Tyr64 side chain, by preventing the Tyr64 side chain to acquire conformation coplanar with the imidazole moiety. The replacement of the phenyl group in the position 143 allowed oxidation and the formation of the red coplanar chromophore.

Positions 66, 106, and 215

To study whether an N-acylimine is formed in mTagBFP, we further mutated amino acid residues that are in close proximity to the N-acylimine in RFPs, such as the conserved among RFPs residues Ser66, Gln106, and Glu215. Earlier, the role of O^{γ} of the Ser69 (corresponding to Ser66 in mTagBFP) side chain in formation of the N-acylimine C = N bond in the DsRed chromophore has been proposed (Sniegowski et al., 2005). The Ser66-Ala substitution resulted in the reduced fluorescence brightness at 456 nm with the absorbance peak at 400 nm (Table 2; Figure S2G). In other words, although the formation of the blue chromophore was deteriorated, it was still possible in the absence of the hydroxyl group of Ser66.

According to the crystal structure of mTagBFP, the $N^{\varepsilon 2}$ atom of Gln106 forms a hydrogen bond with a water molecule that, in turn, makes a hydrogen bond with the N atom of Leu63 (Figure 2B). The Gln106Leu mutation resulted in substantially reduced fluorescence brightness of mTagBFP at 452 nm, with absorbance peak at 400 nm (Table 2; Figure S2H). mTagBFP/Q106L had an additional absorbance maximum at 380 nm. Similarly to the parental mTagBFP, in alkali, the 400 nm maximum converted into the red-shifted 428 nm. In the same conditions, however, the 380 nm peak converted into 379 nm. SDS-PAGE analysis showed that about 50% of the polypeptide chain of the mTagBFP/Q106L mutant was cleaved in the N-acylimine region. We suggest that the absorbance maximum at 380 nm corresponds to the hydrolyzed N-acylimine C = N bond, similar to that observed for denatured DsRed at acidic or alkaline pH (Gross et al., 2000). These data indicate that Gln106Leu substitution reduced efficiency of the N-acylimine formation or its stability.

A catalytic role of Glu215 in the mechanism of the N-acylimine C = N bond formation in the DsRed chromophore has been suggested (Sniegowski et al., 2005). The Glu215Ala substitution in mTagBFP resulted in the complete absence of fluorescence with only a weak absorbance peak at 386 nm, suggesting very inefficient chromophore maturation. Nevertheless, we propose that the formation of the imidazole moiety of the chromophore still occurs. That was also the case for EGFP/E222A (Barondeau et al., 2007) and mKO/E212A (Kikuchi et al., 2008) mutants (equivalent to mTagBFP/E215A variant). Therefore, our data indicate the important role of the Glu215 side chain in the formation of the mTagBFP chromophore. Altogether, these data suggested an existence of an N-acylimine in the mTagBFP chromophore and indicated that the surrounding Ser66, Gln106, and Glu215 residues affect either the N-acylimine formation efficiency or its stability.

Mass-Spectral Analysis of the mTagBFP Chromophore-Bearing Peptide

To confirm the chemical structure of the mTagBFP chromophore, we performed mass-spectral analysis. Denatured mTagBFP was digested by chymotrypsin. The mTagBFP peptide mixture was then desalted and subjected to the mass-spectral analysis. The mass spectrum of mTagBFP chymotrypsin-digested fragments has revealed two monoisotopic masses of 795.4 Da and 1201.6 Da that correspond to chromopeptides. These masses are exactly what would be expected from cyclization (loss of H_2O) and oxidation (loss of H_2) of the chromophore inside the fragments LYGSKTF (cleavage after Phe62 and Phe69) and ATSFLYGSKTF (cleavage after Leu58 and Phe69). Both fragments were separately subjected to further MS/MS fragmentation. The daughter ions for the fragment LYGSKTF are present in Figure 4. Analysis of the MS/MS fragments showed that the dehydrogenation site was located between nitrogen and α-carbon of Leu63. The most prominent peak y_6(I) originated from the cleavage in the vicinity of the N-acylimine C = N bond inside Leu63. The same fragment was observed upon MS/MS fragmentation of the species ATSFLYGSKTF. Fragments with the same cleavage site near the C = N bond were observed in the case of the N-acylimine-containing chromopeptides derived from proteolysis of DsRed (Gross et al., 2000) and chromoprotein gtCP (Martynov et al., 2003). Therefore, mass-spectral data are consistent with the presence of the acylimine C = N bond and with the absence of the double bond between hydroxyphenyl ring of Tyr64 and imidazole-5-ol ring formed by the Leu63-Tyr64-Gly65 tripeptide.

DISCUSSION

An understanding of how specific chemical environments define the distinctive spectral properties of red and blue chromophores might reveal a pathway for their formation. Our data show that TagRFP has the *trans* coplanar anionic chromophore (Figure 1A). The side chains of Asn143 and Ser158 make hydrogen bonds with the hydroxyl of the hydroxyphenyl moiety (Figure 2A). These two hydrogen bonds, together with the π−π interaction between the hydroxyphenyl group and His197, are probably the most

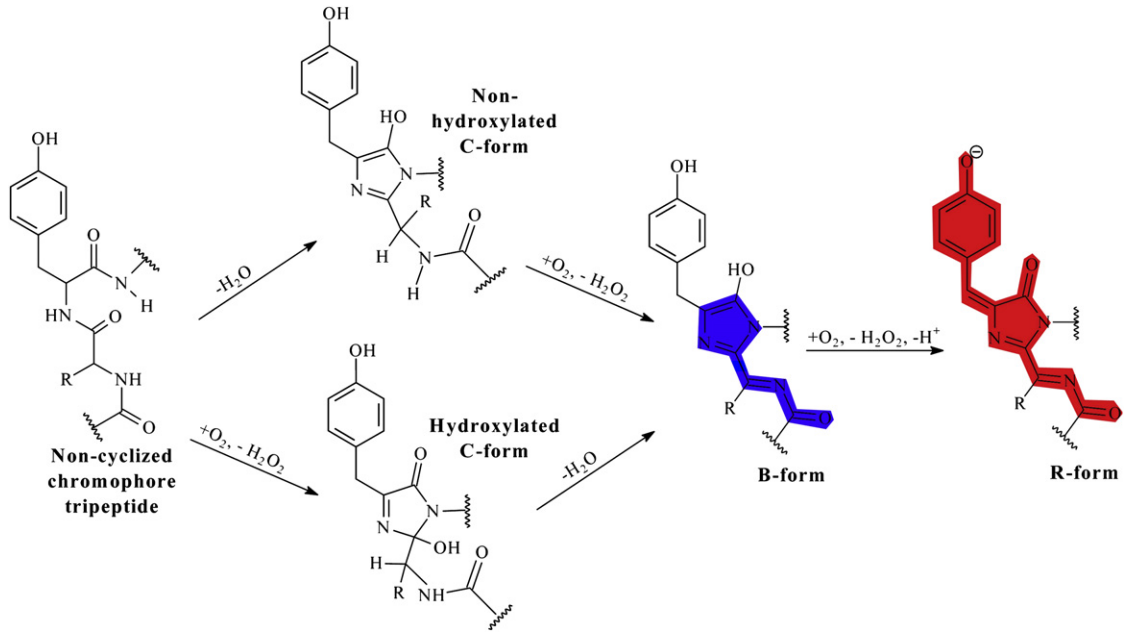

Figure 5. Proposed Pathways for the Formation of the mTagBFP and TagRFP Chromophores
The C-form is the chromophore precursor, the B-form is the blue-emitting chromophore form, and the R-form is the red-emitting chromophore form.

important determinants for stabilizing the hydroxyphenyl moiety in a *trans* coplanar anionic configuration. It has been shown in eqFP611 (Nienhaus et al., 2008) and mKate (Pletnev et al., 2008) that *trans* or *cis* anionic configurations of the chromophore are determined by residues 143 and 158. When serine was introduced at the position 143, a *cis* configuration was stabilized, and when serine was introduced at the position 158, a *trans* configuration was stabilized.

The comparison of TagRFP and mTagBFP structures, as well as the analysis of mTagBFP/F143S mutant, revealed the main driving force favoring the formation of the blue chromophore in mTagBFP. Phe143 pushes the hydroxyphenyl group of Tyr64 out of the plane of the imidazole-5-ol ring and prevents the formation of the C^{α}-C^{β} double bond in the Tyr64 side chain. We suggest a chemical structure of the mTagBFP chromophore (B-form) and mechanism of its formation in Figure 5. The structure is based on several lines of evidence. First, the electron density in the mTagBFP crystal is consistent with the mainly planar geometry of Leu63 C^{α} and tetrahedral geometry of Tyr64 C^{β}. This implies that the N-acylimine is possibly present in the mTagBFP chromophore; however, there is no oxidation of the C^{α}-C^{β} bond in the Tyr64 side chain. Moreover, electron density indicates mainly planar geometry of the Tyr64 C^{α} and coplanar imidazole ring with the C = N acylimine bond. This observation suggests that mTagBFP contains the imidazole-5-ol but not the imidazolone in its chromophore. Second, the mTagBFP denaturation in alkali or acid resulted in the absorbance spectra that are not characteristic of the GFP-like or DsRed-like chromophores (Figure 3B), which contain the C^{α}-C^{β} double bond in the Tyr64 side chain. Third, mutagenesis of Ser66, Gln106, and Glu215 surrounding the N-acylimine influenced either formation or stability of the N-acylimine C = N bond. Moreover, mTagBFP and its mutants with the aliphatic residues at position 64 had almost identical absorbance and emission spectra. This confirms that there is no C^{α}-C^{β} double bond in the Tyr64 side chain. Lastly, the mass spectrum analysis provides the mass of the chromophore-bearing peptide to be 20 Da less than that calculated from the amino acid content. Tandem mass spectrometry indicates that the dehydrogenation site in the mTagBFP chromophore is located between N and C^{α} of Leu63, which is similar to the site of the N-acylimine C = N bond in the DsRed-like chromophore. Altogether, these data are in agreement with *N*-[(5-hydroxy-1*H*-imidazole-2-yl)methylidene]acetamide, which we propose to be the mTagBFP chromophore (B-form in Figure 5).

It has been suggested that the first step in maturation of a DsRed chromophore is the formation of the GFP-like chromophore containing the C^{α}-C^{β} double bond in the Tyr64 side chain (Gross et al., 2000; Yarbrough et al., 2001). The second step involves an oxidation of the bond between the C^{α} and N of the first amino acid in the chromophore tripeptide to form the N-acylimine. The crystallographic analysis, mass spectrometry data and properties of the site-specific mutants allowed for the proposal of a hypothetical chemical pathway for the formation of the TagRFP chromophore (R-form) (Figure 5). The key feature of the pathway is that the formation of the N-acylimine C = N bond precedes the oxidation of the C^{α}-C^{β} bond in the Tyr64 side chain. It is in agreement with the observation that the DsRed-like red chromophores are formed after the blue-emitting precursors (Verkhusha et al., 2004) and with the chemical structure of the mTagBFP blue chromophore discussed above.

There are two possible pathways for the B-form formation (Figure 5). In one pathway, the first step consists of cyclization of the chromophore tripeptide, followed by dehydration, resulting in the formation of a colorless nonhydroxylated C-form. The next oxidation step results in the formation of an N-acylimine containing the blue-emitting chromophore (B-form). In an

alternative pathway for the B-form formation, the oxidation step precedes dehydration of the tripeptide. Oxidation results in the formation of the hydroxylated C-form. Dehydration of the hydroxylated C-form can then occur with the formation of the B-form. It has been shown for GFP maturation that the oxidation reaction, accompanied by the hydrogen peroxide release, takes place before the chromophore dehydration (Zhang et al., 2006) that is similar to the second proposed pathway. Further oxidation of the C^{α}-C^{β} bond in the Tyr64 side chain of the B-form results in the formation of the red chromophore (R-form).

We suggest that the formation pathway for the TagRFP's red chromophore via the mTagBFP-like intermediate proposed in this work may also occur in other RFPs (Piatkevich and Verkhusha, 2010). This suggestion is based on several observations. First, the blue intermediates have been observed in the courses of maturation of many RFPs and red-shifted CPs (Verkhusha et al., 2004; Wilmann et al., 2005). Second, several Fluorescent Timer proteins, which change color from blue to red over time, were developed from mCherry RFP (Subach et al., 2009; Pletnev et al., 2010). Lastly, several BFPs have been obtained by introducing the similar mutations into RFPs of different genetic background (Subach et al., 2008).

A model for the formation of the red chromophore via a GFP-like intermediate has been suggested on the basis of the observation of green- and red-emitting species in DsRed (Gross et al., 2000). Later, however, it was shown that the GFP-like chromophore is not an intermediate in the maturation pathway of the DsRed-like red chromophore but the dead-end product (Verkhusha et al., 2004). A possible reason why the red chromophore can not formed from the green intermediate is that the GFP-like chromophore is anionic (Niwa et al., 1996). A carbanion state has been proposed for the formation pathway of the DsRed-like chromophore (Yarbrough et al., 2001). However, formation of the carbanion from the anionic GFP-like chromophore is energetically unfavorable. In contrast, the proposed mTagBFP-like chromophore does not contain a negative charge and allows formation of its carbanion derivative; consequently, the DsRed-like red fluorescent chromophore can be formed from it.

Figure 5 can be expanded further to explain formation of different fluorescent colors observed in FPs. After cyclization of the chromophore-bearing tripeptide, there are two chemical pathways. The first one is the formation of the N-acylimine, and the second one is oxidation of the C^{α}-C^{β} bond in the Tyr64 side chain. These two reactions are competitive processes. In GFPs, reaction of the Tyr64 C^{α}-C^{β} bond dehydrogenation occurs first and results in the anionic GFP-like chromophore (Niwa et al., 1996). The second oxidation, which leads to the N-acylimine formation, becomes energetically unfavorable. It can occur, nevertheless, with a GFP-like chromophore in an excited state in the presence of a strong oxidant (Bogdanov et al., 2009). In contrast, in RFPs, the N-acylimine formation occurs first, followed by oxidation of the C^{α}-C^{β} bond in Tyr64. In BFPs with Tyr in the chromophore-forming tripeptide, the chemical transformations are stopped right after the N-acylimine formation.

SIGNIFICANCE

In this work, the crystal structures of the red fluorescent protein TagRFP and its blue variant mTagBFP have been determined. On the basis of the crystal structure, mass spectra, and analysis of the site-specific mutants, we have shown that mTagBFP has a type of the chromophore, which contains the N-acylimine but does not have the C^{α}-C^{β} double bond in the Tyr64 side chain. We have proposed the chemical pathway for the formation of the DsRed-like chromophore, such as that observed in TagRFP via the mTagBFP-like intermediate. This pathway may provide a basis for the rational design of FPs with novel spectral and photophysical properties and for the development of molecular FP-based biosensors.

EXPERIMENTAL PROCEDURES

Cloning, Expression, and Protein Purification

For bacterial expression of TagRFP, the pBAD/HisB vector (Invitrogen) was modified by inserting the DNA sequence of the Tobacco Etch Virus (TEV) protease site (-ENLYPQG- amino acids) (Carrington and Dougherty, 1988) between the BglII site and the sequence encoding His_6-tag. The polymerase chain reaction (PCR) amplified BglII/EcoRI fragment encoding TagRFP was then cloned into the modified pBAD/HisB. The recombinant TagRFP protein with the N-terminal His_6-tag was expressed in the LMG194 bacterial strain (Invitrogen) by overnight culture in RM minimal medium at 37°C in the presence of 0.005% arabinose. The culture was then centrifuged at 5,000 rpm at 4°C for 15 min; the cell pellet was resuspended in 50 mM NaH_2PO_4 and 300 mM NaCl buffer (pH 8.0) and was lysed by sonication on ice. The recombinant protein was purified with Ni-NTA resin (QIAGEN) followed by dialysis for 3 hr against the TEV protease cleavage buffer consisting of 50 mM Tris-HCl, 1 mM EDTA, 1 mM DTT, and 150 mM NaCl (pH 7.5). The His_6-tag was cleaved with TEV protease at a TagRFP:TEV protease ratio of 10:1 at room temperature for 20 hr. The released TagRFP was dialysed against 10 mM NaH_2PO_4 (pH 6.0), followed by purification with cation-exchange chromatography using SP-sepharose (GE Healthcare).

For bacterial expression of mTagBFP, the pBAD/HisB vector (Invitrogen) was modified by shortening the N-terminal His_6-tag to the MGSHHHHHHGRS- amino acids. The PCR-amplified BglII/EcoRI fragment encoding mTagBFP was cloned into the modified pBAD/HisB vector and expressed in LMG194 host (Invitrogen). The bacterial culture in RM minimal medium supplemented with 0.005% arabinose was grown overnight at 37°C. The culture was centrifuged at 5,000 rpm at 4°C for 15 min. The cell pellet was resuspended in 50 mM NaH_2PO_4 and 300 mM NaCl buffer (pH 8.0) and was lysed by sonication on ice. The recombinant protein was purified using Ni-NTA resin (QIAGEN) followed by dialysis for 3 hr against 10 mM NaH_2PO_4 (pH 6.0). The mTagBFP protein was then purified by cation-exchange chromatography using the SP-sepharose (GE Healthcare).

Protein Crystallization

Before crystallization, TagRFP protein without His_6-tag and mTagBFP protein containing a short N-terminal His_6-tag were dialyzed against 10 mM Tris-HCl and 100 mM NaCl (pH 8.0) and were concentrated to 15 mg/ml using the 3,000 MWCO Amicon (Millipore) centrifugal concentrator. Diffraction quality crystals were grown using the sitting drop vapor diffusion method by mixing 1 μl of protein and 1 μl of reservoir solution and equilibrating the samples against reservoir solution. For TagRFP, the reservoir solution contained 30% PEG 4000, 0.1 M Tris-HCl (pH 8.5), 0.2 M $MgCl_2$, and 0.1 M TCEP. Diffraction from the TagRFP crystals was consistent with the space group $I4_1$ with unit cell dimensions a = b = 130.99 Å, c = 105.97 Å, $\alpha = \beta = \gamma = 90°$, and four TagRFP chains in the asymmetric unit. In the case of mTagBFP, the reservoir solution contained 2.0 M ammonium sulfate. Diffraction was consistent with the space group $P2_12_12_1$, with unit cell dimensions a = 82.95 Å, b = 105.94 Å, c = 137.16 Å, $\alpha = \beta = \gamma = 90°$, and four mTagBFP chains in the asymmetric unit.

X-Ray Diffraction Data Collection and Crystallographic Refinement

Crystals of TagRFP with dimensions 0.05 × 0.05 × 0.4 mm^3 were mounted in cryo-loops directly from the crystallization droplet and flash-cooled in liquid nitrogen. Prior to freezing, 1 μl of 2 M lithium sulfate was added

(as cryo-protectant) to the droplets containing mTagBFP crystals, and then crystals were flash-cooled in liquid nitrogen. Diffraction data were collected on a Quantum 315 CCD detector (Area Detector Systems Corporation) with 1.08 Å wavelength radiation on the X29A beamline (National Synchrotron Light Source). Intensities were integrated using the program HKL2000 and reduced to amplitudes using the program TRUNCATE (see Table 1 for statistics) (Otwinowski and Minor, 1997; Storoni et al., 2004). The structures were determined using the molecular replacement method with PHASER (CCP4, 1994). Model building and refinement were performed with the programs REFMAC and COOT (Storoni et al., 2004; Emsley and Cowtan, 2004). The quality of the final structure was verified with composite omit maps, and the stereochemistry was checked with the programs WHATCHECK (Hooft et al., 1996) and PROCHEK (Laskowski et al., 1993). The LSQKAB and SSM algorithms were used for structural superimpositions (Storoni et al., 2004; Krissinel and Henrick, 2004). Quaternary structures were analyzed using the PISA server (Krissinel and Henrick, 2007). No rotational order-disorder structure was observed (Pletnev et al., 2009).

Mutagenesis of mTagBFP and TagRFP

mTagBFP mutants were produced by site-directed mutagenesis using the mTagBFP gene in the pBAD/HisB vector as the templates. The mutant proteins were expressed in LMG host (Invitrogen) and purified as described above for mTagBFP.

Spectroscopy

Absorbance spectra were recorded on a U-3010 spectrophotometer (Hitachi). The excitation and emission spectra were measured using a FluoroMax-3 spectrofluorometer (Jobin Yvon). For measurements the protein samples in phosphate buffered saline (PBS) were used. Absorbance and fluorescence of acid- or alkali-denatured FPs were measured right after the mixing of the protein sample with HCl (to the final concentration of 0.2 M) or NaOH (to the final concentration of 0.7 M) in the optical cuvette. Brightness of proteins was calculated as a product of quantum yield and extinction coefficient. Quantum yield was measured using mTagBFP (quantum yield is 0.63; Subach et al., 2008) or TagRFP (quantum yield is 0.48; Merzlyak et al., 2007) as the reference standards, respectively. Protein concentrations used in the calculation of extinction coefficients were determined by the BCA assay (Pierce).

Enzymatic Proteolysis

Aliquot of 20 μg of His_6-tagged mTagBFP was reduced with 5 mM DTT and alkylated with 10 mM iodoacetamide and then subjected to an in-solution digestion with chymotrypsin, as described elsewhere (Gross et al., 2000). The sample was evaporated to near dryness in a Speedvac and resuspended in 3 μl of 6 M guanidinium chloride and heated to 80°C for 30 s. The sample was cooled to room temperature, and 1.0 μl of 0.33 M hydrochloric acid was added to neutralize the digestion buffer; 30 μl of chymotrypsin buffer containing 0.1 M Tris-HCl (pH 7.8) and 10 mM $CaCl_2$ was added, and then chymotrypsin was added at an enzyme:protein ratio of 1:60. The digests were incubated at room temperature for 22 hr and quenched with 0.1% TFA. The peptides were desalted and isolated using a C18 ZipTip (Millipore).

Peptide Analysis

The chymotryptic peptides were mixed (1:1) with α-cyano-4-hydroxycinnamic acid solution (50% acetonitrile and water containing 0.1% tri-fluoroacetic acid). An aliquot of 1 μl of the mixture was put on a MALDI target and air-dried. Mass spectra were acquired on a 4800 MALDI TOF/TOF mass spectrometer (Applied Biosystems). The instrument was equipped with a Nd:YAG laser (PowerChip, JDS Uniphase) operating at 200 Hz and controlled by Applied Biosystems 4000 Series Explorer version 3.6 software. Each spectrum was accumulated with 500 shots in positive ion mode. MS/MS were acquired in PSD mode with mass isolation window ±3 Da.

ACCESSION NUMBERS

The atomic coordinates and structural factors have been deposited in the Protein Data Bank (entry 3M22 for TagRFP and entry 3M24 for mTagBFP).

SUPPLEMENTAL INFORMATION

Supplemental Information includes two figures, Supplemental Experimental Procedures, and Supplemental References and can be found with this article online at doi:10.1016/j.chembiol.2010.03.005.

ACKNOWLEDGMENTS

This work was supported by the National Institutes of Health (grant GM073913 to V.V.V.) and by the Albert Einstein Cancer Center. We thank H.Xiao for measuring mass spectra and U. Ramagopal for assistance with structure determination. We also thank the staff of the X29 beamline at the National Synchrotron Light Source, Brookhaven National Laboratory.

Received: December 9, 2009
Revised: January 23, 2010
Accepted: March 5, 2010
Published: April 22, 2010

REFERENCES

Andresen, M., Wahl, M.C., Stiel, A.C., Gräter, F., Schäfer, L.V., Trowitzsch, S., Weber, G., Eggeling, C., Grubmüller, H., Hell, S.W., and Jakobs, S. (2005). Structure and mechanism of the reversible photoswitch of a fluorescent protein. Proc. Natl. Acad. Sci. USA *102*, 13070–13074.

Barondeau, D.P., Kassmann, C.J., Tainer, J.A., and Getzoff, E.D. (2007). The case of the missing ring: radical cleavage of a carbon-carbon bond and implications for GFP chromophore biosynthesis. J. Am. Chem. Soc. *129*, 3118–3126.

Bogdanov, A.M., Mishin, A.S., Yampolsky, I.V., Belousov, V.V., Chudakov, D.M., Subach, F.V., Verkhusha, V.V., Lukyanov, S., and Lukyanov, K.A. (2009). Green fluorescent proteins are light-induced electron donors. Nat. Chem. Biol. *5*, 459–461.

Brejc, K., Sixma, T.K., Kitts, P.A., Kain, S.R., Tsien, R.Y., Ormö, M., and Remington, S.J. (1997). Structural basis for dual excitation and photoisomerization of the *Aequorea victoria* green fluorescent protein. Proc. Natl. Acad. Sci. USA *94*, 2306–2311.

Bulina, M.E., Verkhusha, V.V., Staroverov, D.B., Chudakov, D.M., and Lukyanov, K.A. (2003). Hetero-oligomeric tagging diminishes non-specific aggregation of target proteins fused with Anthozoa fluorescent proteins. Biochem. J. *371*, 109–114.

Carrington, J.C., and Dougherty, W.G. (1988). A viral cleavage site cassette: identification of amino acid sequences required for tobacco etch virus polyprotein processing. Proc. Natl. Acad. Sci. USA *85*, 3391–3395.

CCP4 (Collaborative Computational Project, Number 4). (1994). The CCP4 suite: programs for protein crystallography. Acta Crystallogr. D Biol. Crystallogr. *50*, 760–763.

Emsley, P., and Cowtan, K. (2004). Coot: model-building tools for molecular graphics. Acta Crystallogr. D Biol. Crystallogr. *60*, 2126–2132.

Gross, L.A., Baird, G.S., Hoffman, R.C., Baldridge, K.K., and Tsien, R.Y. (2000). The structure of the chromophore within DsRed, a red fluorescent protein from coral. Proc. Natl. Acad. Sci. USA *97*, 11990–11995.

Heim, R., and Tsien, R.Y. (1996). Engineering green fluorescent protein for improved brightness, longer wavelengths and fluorescence energy transfer. Curr. Biol. *6*, 178–182.

Heim, R., Prasher, D.C., and Tsien, R.Y. (1994). Wavelength mutations and posttranslational autooxidation of green fluorescent protein. Proc. Natl. Acad. Sci. USA *91*, 12501–12504.

Hooft, R.W., Vriend, G., Sander, C., and Abola, E.E. (1996). Errors in protein structures. Nature *381*, 272.

Kikuchi, A., Fukumura, E., Karasawa, S., Mizuno, H., Miyawaki, A., and Shiro, Y. (2008). Structural characterization of a thiazoline-containing chromophore in an orange fluorescent protein, monomeric Kusabira Orange. Biochemistry *47*, 11573–11580.

Kogure, T., Karasawa, S., Araki, T., Saito, K., Kinjo, M., and Miyawaki, A. (2006). A fluorescent variant of a protein from the stony coral Montipora facilitates dual-color single-laser fluorescence cross-correlation spectroscopy. Nat. Biotechnol. *24*, 577–581.

Krissinel, E., and Henrick, K. (2004). Secondary-structure matching (SSM), a new tool for fast protein structure alignment in three dimensions. Acta Crystallogr. D Biol. Crystallogr. *60*, 2256–2268.

Krissinel, E., and Henrick, K. (2007). Inference of macromolecular assemblies from crystalline protein state. J. Mol. Biol. *372*, 774–797.

Laskowski, R., MacArthur, M., Moss, D., and Thornton, J. (1993). PROCHECK: a program to check the stereochemical quality of protein structures. J. Appl. Cryst. *26*, 283–291.

Martynov, V.I., Maksimov, B.I., Martynova, N.Y., Pakhomov, A.A., Gurskaya, N.G., and Lukyanov, S.A. (2003). A purple-blue chromoprotein from *Goniopora tenuidens* belongs to the DsRed subfamily of GFP-like proteins. J. Biol. Chem. *278*, 46288–46292.

Merzlyak, E.M., Goedhart, J., Shcherbo, D., Bulina, M.E., Shcheglov, A.S., Fradkov, A.F., Gaintzeva, A., Lukyanov, K.A., Lukyanov, S., Gadella, T.W., and Chudakov, D.M. (2007). Bright monomeric red fluorescent protein with an extended fluorescence lifetime. Nat. Methods *4*, 555–557.

Nienhaus, K., Nar, H., Heilker, R., Wiedenmann, J., and Nienhaus, G.U. (2008). Trans-cis isomerization is responsible for the red-shifted fluorescence in variants of the red fluorescent protein eqFP611. J. Am. Chem. Soc. *130*, 12578–12579.

Niwa, H., Inouye, S., Hirano, T., Matsuno, T., Kojima, S., Kubota, M., Ohashi, M., and Tsuji, F.I. (1996). Chemical nature of the light emitter of the Aequorea green fluorescent protein. Proc. Natl. Acad. Sci. USA *93*, 13617–13622.

Ormö, M., Cubitt, A.B., Kallio, K., Gross, L.A., Tsien, R.Y., and Remington, S.J. (1996). Crystal structure of the *Aequorea victoria* green fluorescent protein. Science *273*, 1392–1395.

Otwinowski, W., and Minor, F. (1997). Processing of X-ray diffraction data collected in oscillation mode. Methods Enzymol. *276*, 307–326.

Petersen, J., Wilmann, P.G., Beddoe, T., Oakley, A.J., Devenish, R.J., Prescott, M., and Rossjohn, J. (2003). The 2.0 Å crystal structure of eqFP611, a far red fluorescent protein from the sea anemone Entacmaea quadricolor. J. Biol. Chem. *278*, 44626–44631.

Piatkevich, K.D., and Verkhusha, V.V. (2010). Advances in engineering of fluorescent proteins and photoactivatable proteins with red emission. Curr. Opin. Chem. Biol. *14*, 23–29.

Pletnev, S., Shcherbo, D., Chudakov, D., Pletneva, N., Merzlyak, E., Wlodawer, A., Dauter, Z., and Pletnev, V. (2008). A crystallographic study of bright far-red fluorescent protein mKate reveals pH-induced cis-trans isomerization of the chromophore. J. Biol. Chem. *283*, 28980–28987.

Pletnev, S., Morozova, K.S., Verkhusha, V.V., and Dauter, Z. (2009). Rotational order-disorder structure of fluorescent protein FP480. Acta Crystallogr. D Biol. Crystallogr. *65*, 906–912.

Pletnev, S., Subach, F.V., Dauter, Z., Wlodawer, A., and Verkhusha, V.V. (2010). Understanding blue-to-red conversion in monomeric fluorescent timers and hydrolytic degradation of their chromophores. J. Am. Chem. Soc. *132*, 2243–2253.

Prescott, M., Ling, M., Beddoe, T., Oakley, A.J., Dove, S., Hoegh-Guldberg, O., Devenish, R.J., and Rossjohn, J. (2003). The 2.2 Å crystal structure of a pocilloporin pigment reveals a nonplanar chromophore conformation. Structure *11*, 275–284.

Quillin, M.L., Anstrom, D.M., Shu, X., O'Leary, S., Kallio, K., Chudakov, D.M., and Remington, S.J. (2005). Kindling fluorescent protein from *Anemonia sulcata*: dark-state structure at 1.38 Å resolution. Biochemistry *44*, 5774–5787.

Shu, X., Shaner, N.C., Yarbrough, C.A., Tsien, R.Y., and Remington, S.J. (2006). Novel chromophores and buried charges control color in mFruits. Biochemistry *45*, 9639–9647.

Sniegowski, J.A., Lappe, J.W., Patel, H.N., Huffman, H.A., and Wachter, R.M. (2005). Base catalysis of chromophore formation in Arg96 and Glu222 variants of green fluorescent protein. J. Biol. Chem. *280*, 26248–26255.

Stepanenko, O.V., Verkhusha, V.V., Kuznetsova, I.M., Uversky, V.N., and Turoverov, K.K. (2008). Fluorescent proteins as biomarkers and biosensors: throwing color lights on molecular and cellular processes. Curr. Protein Pept. Sci. *9*, 338–369.

Stiel, A.C., Trowitzsch, S., Weber, G., Andresen, M., Eggeling, C., Hell, S.W., Jakobs, S., and Wahl, M.C. (2007). 1.8 Å bright-state structure of the reversibly switchable fluorescent protein Dronpa guides the generation of fast switching variants. Biochem. J. *402*, 35–42.

Storoni, L.C., McCoy, A.J., and Read, R.J. (2004). Likelihood-enhanced fast rotation functions. Acta Crystallogr. D Biol. Crystallogr. *60*, 432–438.

Subach, O.M., Gundorov, I.S., Yoshimura, M., Subach, F.V., Zhang, J., Grünwald, D., Souslova, E.A., Chudakov, D.M., and Verkhusha, V.V. (2008). Conversion of red fluorescent protein into a bright blue probe. Chem. Biol. *15*, 1116–1124.

Subach, F.V., Subach, O.M., Gundorov, I.S., Morozova, K.S., Piatkevich, K.D., Cuervo, A.M., and Verkhusha, V.V. (2009). Monomeric fluorescent timers that change color from blue to red report on cellular trafficking. Nat. Chem. Biol. *5*, 118–126.

Verkhusha, V.V., Chudakov, D.M., Gurskaya, N.G., Lukyanov, S., and Lukyanov, K.A. (2004). Common pathway for the red chromophore formation in fluorescent proteins and chromoproteins. Chem. Biol. *11*, 845–854.

Wilmann, P.G., Petersen, J., Pettikiriarachchi, A., Buckle, A.M., Smith, S.C., Olsen, S., Perugini, M.A., Devenish, R.J., Prescott, M., and Rossjohn, J. (2005). The 2.1 Å crystal structure of the far-red fluorescent protein HcRed: inherent conformational flexibility of the chromophore. J. Mol. Biol. *349*, 223–237.

Wilmann, P.G., Turcic, K., Battad, J.M., Wilce, M.C., Devenish, R.J., Prescott, M., and Rossjohn, J. (2006). The 1.7 Å crystal structure of Dronpa: a photoswitchable green fluorescent protein. J. Mol. Biol. *364*, 213–224.

Yarbrough, D., Wachter, R.M., Kallio, K., Matz, M.V., and Remington, S.J. (2001). Refined crystal structure of DsRed, a red fluorescent protein from coral, at 2.0 Å resolution. Proc. Natl. Acad. Sci. USA *98*, 462–467.

Zhang, L., Patel, H.N., Lappe, J.W., and Wachter, R.M. (2006). Reaction progress of chromophore biogenesis in green fluorescent protein. J. Am. Chem. Soc. *128*, 4766–4772.